MCB
Journals.ASM.org

# NF-E2 p45 Is Important for Establishing Normal Function of Platelets

**Rie Fujita,[a] Mariko Takayama-Tsujimoto,[a] Hironori Satoh,[a] Laura Gutiérrez,[b] Hiroyuki Aburatani,[c] Satoshi Fujii,[d] Akinori Sarai,[d] Emery H. Bresnick,[e] Masayuki Yamamoto,[a] Hozumi Motohashi[f]**

Department of Medical Biochemistry, Tohoku University Graduate School of Medicine, Sendai, Japan[a]; Department of Blood Cell Research, Sanquin Research and Landsteiner Laboratory, Academic Medical Center, University of Amsterdam, Amsterdam, The Netherlands[b]; Research Center for Advanced Science and Technology, University of Tokyo, Tokyo, Japan[c]; Department of Bioscience and Bioinformatics, Kyushu Institute of Technology, Iizuka, Japan[d]; UW—Madison Blood Research Program, Paul Carbone Comprehensive Cancer Center, Department of Cell and Regenerative Biology, University of Wisconsin School of Medicine and Public Health, Madison, Wisconsin, USA[e]; Department of Gene Expression Regulation, Institute of Development, Aging and Cancer, Tohoku University, Sendai, Japan[f]

**NF-E2 is a heterodimeric transcription factor consisting of p45 and small Maf subunits. Since *p45*$^{-/-}$ mice display severe thrombocytopenia, p45 is recognized as a critical regulator of platelet production from megakaryocytes. To identify direct p45 target genes in megakaryocytes, we used chromatin immunoprecipitation (ChIP) sequencing to analyze the genome-wide chromatin occupancy of p45 in primary megakaryocytes. p45 target gene candidates obtained from the analysis are implicated in the production and function of platelets. Two of these genes, *Selp* and *Myl9*, were verified as direct p45 targets through multiple approaches. Since P-selectin, encoded by *Selp*, plays a critical role in platelet function during thrombogenesis, we tested whether p45 determines the intrinsic reactivity and potency of platelets generated from megakaryocytes. Mice expressing a hypomorphic p45 mutant instead of wild-type p45 in megakaryocytes (*p45*$^{-/-}$:ΔNTD-Tg mice) displayed platelet hypofunction accompanied by mild thrombocytopenia. Furthermore, lung metastasis of melanoma cells, which requires platelet activation, was repressed in *p45*$^{-/-}$:ΔNTD-Tg mice compared to control mice, validating the impaired function of platelets produced from *p45*$^{-/-}$:ΔNTD-Tg megakaryocytes. By activating genes in megakaryocytes that mediate platelet production and function, p45 determines the quantity and quality of platelets.**

Platelets are anucleate blood cells that play a central role in the processes of hemostasis and thrombosis. Equipped with highly organized cytoskeletons, unique receptors, and specialized secretory granules, circulating platelets respond to blood vessel injury by changing shape, secreting granule contents, and aggregating (1). These responses are advantageous for hemostasis but can be detrimental when they cause tissue ischemia or infarction. Accordingly, establishing and maintaining normal platelet number and activity is essential for health.

In addition to their hemostatic function, recent studies revealed that platelets are involved in atherosclerosis, cancer metastasis, immune responses, and inflammation (2–9). Although it is well established that extrinsic factors, such as coagulation factors and vascular endothelial cells, have a major influence on platelet function (10, 11), factors intrinsic to platelets are also crucial for the platelet response and subsequent pathological conditions. As platelets are a rich source of chemokines, cytokines, and growth factors (9, 12–14), the impact of platelet degranulation on the surrounding environment depends on the integrity of platelet functions. Most of the bioactive substances are preformed and packed into different subsets of granules already present in megakaryocytes from which platelets are generated. Thus, proper gene expression in the terminal maturation stage of megakaryocytes is required to establish functional platelets. Although many questions remain unanswered regarding mechanisms underlying the transcriptional control of genes mediating platelet function, the NF-E2 transcription factor is considered to be an essential transcriptional regulator in megakaryocytes.

NF-E2 is a heterodimeric transcription activator composed of p45 and small Maf subunits. Both subunits possess a typical basic region-leucine zipper (bZip) motif that binds to a consensus sequence called the NF-E2 motif (GC TGA G/C TCA T) (15). p45 possesses a transcription activation domain in the N-terminal region (16, 17) and belongs to the CNC protein family, which includes Nrf1, Nrf2, and Nrf3 (18). Small Maf is a common heterodimeric partner of the CNC family proteins and is essential for DNA binding. A well-characterized feature of the DNA recognition sequence by Maf-containing dimers, including NF-E2, is the presence of the GC dinucleotides in the flanking portion of the AP-1 consensus motif (TGA G/C TCA) (19–21). Small Maf does not have canonical activation or repression domains, but it does have important roles in transcriptional regulation besides determining the DNA recognition specificity of NF-E2. Sumoylation of small Maf mediates active repression (22), and its C-terminal region targets NF-E2 to a subnuclear region permissive for active transcription (23).

Genetic evidence has demonstrated critical contributions of p45 and small Maf to the terminal maturation of megakaryocytes and platelet production. *p45*$^{-/-}$ mice and small Maf mutant mice display severe thrombocytopenia, and most of these mice die by fatal hemorrhage before weaning (24, 25). In both mutants, mature polyploid megakaryocytes accumulate in the bone marrow and spleen, and the formation of proplatelets from megakaryo-

**Received** 18 September 2012 **Returned for modification** 11 October 2012
**Accepted** 29 April 2013

**Published ahead of print** 6 May 2013

Address correspondence to Masayuki Yamamoto, masiyamamoto@med.tohoku.ac.jp, or Hozumi Motohashi, hozumim@idac.tohoku.ac.jp.

Supplemental material for this article may be found at http://dx.doi.org/10.1128/MCB.01274-12.



doi:10.1128/MCB.01274-12

cytes is completely inhibited, suggesting that NF-E2 is essential during the late stages of megakaryopoiesis (26, 27). Several genes, such as *Thromboxane synthase* (*Txs*), β*1 Tubulin*, *Rab27b*, and *Lims1* (28–31), have been identified as p45 target genes in megakaryocytes.

To better understand the function of p45 during megakaryopoiesis, we combined chromatin immunoprecipitation sequencing (ChIP-Seq) and microarray analyses in primary megakaryocytes to establish the direct p45 target gene ensemble. The typical NF-E2 binding sequence (GC TGA G/C TCA T/C) was enriched in the p45 binding peaks. Among the genes that were downregulated in *p45*-null megakaryocytes, 49 genes were identified as p45 target gene candidates that were directly activated by p45 through NF-E2 motifs. Among these genes, 15 were implicated previously in regulating platelet function (referred to as platelet genes), suggesting that p45 confers important platelet activities. Further validation utilizing multiple criteria identified two platelet genes, *Selp* and *Myl9*, as direct NF-E2 targets. To test the contribution of p45-mediated transcriptional activation to the establishment of platelet function, we analyzed mice expressing a p45 deletion mutant (ΔNTD), which lacks part of the established transactivation domain in megakaryocytes, instead of endogenous p45 ($p45^{-/-}$:ΔNTD-Tg mice). $p45^{-/-}$:ΔNTD-Tg mice displayed mild thrombocytopenia accompanied by platelet hypofunction, which was associated with reduced expression of the platelet genes. Importantly, we discovered that lung metastasis of melanoma cells, which requires proper platelet activation, was suppressed in $p45^{-/-}$:ΔNTD-Tg mice, indicating that reduced p45 activity in megakaryocytes impairs crucial platelet functions *in vivo*. Our results provide strong evidence that p45 is essential for establishing normal platelet function as well as for generating the requisite number of platelets.

## MATERIALS AND METHODS

**Mice.** $p45^{-/-}$, $MafG^{-/-}$, $MafK^{-/-}$, p45-TG, and ΔNTD-Tg mice were generated and characterized as described previously (17, 25, 32). Compound mutant ($p45^{-/-}$:p45-TG and $p45^{-/-}$:ΔNTD-Tg) mice were generated on a C57BL/6 background after backcrossing for three generations. The xenograft experiment using B16-F10 melanoma cell-derived B16-F10-td-Tomato cells was described previously (33). Mice were intravenously injected with $1 \times 10^6$ B16-F10-td-Tomato cells in a total volume of 0.2 ml phosphate-buffered saline. The whole lung was dissected 18 days after the inoculation of B16-F10-td-Tomato cells, and macroscopically observable metastatic nodules were counted. The experimental procedures were approved by the Animal Center of Tohoku University, and the experiments were conducted in accordance with the Regulation for Animal Experiments of Tohoku University.

**Primary culture of megakaryocytes.** Whole livers were collected from mouse fetuses at embryonic day 13.5 (E13.5), and single-cell suspensions were prepared by successive passage through 25-gauge needles. The fetal liver cells were maintained in RPMI 1640 (Wako, Osaka, Japan) supplemented with 20% charcoal-stripped fetal bovine serum (FBS), 100 U/ml penicillin, 100 μg/ml streptomycin, and 50 ng/ml recombinant human thrombopoietin (TPO) (generously provided by Kyowa Hakko Kirin Co. Ltd., Tokyo, Japan). Megakaryocytes were harvested for RNA purification and chromatin immunoprecipitation (ChIP) assay from a day 3 culture. All of the samples processed from primary megakaryocytes were compared among littermates.

**Microarray analysis.** The transcriptome was compared between wild-type (WT) and $p45^{-/-}$ megakaryocytes in biological triplicates using microarray analysis. $CD41^+$ cells were enriched using a biotinylated anti-CD41 antibody (clone MWReg30; Serotec, Raleigh, NC) and streptavidin-coupled Dynabeads (Dynal Biotech ASA, Oslo, Norway) from a culture of E13.5 fetal liver cells of WT and $p45^{-/-}$ mice. The total RNA purified from the sorted $CD41^+$ cells was processed and hybridized to a 4×44K whole-mouse-genome microarray (Agilent Technologies, Santa Clara, CA). The experimental procedures for GeneChip were performed according to the manufacturer's protocol. The arrays were scanned using the G2539A microarray scanner system (Agilent Technologies), and the resulting data were analyzed using the Limma package (34) of open-source R statistical software (35) with Bioconductor (36). We performed a model-based background correction using the Limma function normexp with the option offset set to 25 (37), and we performed between-array normalization by the quantile method (38). We filtered the data from the probes for which none of the six samples showed high fluorescence intensity (above 100 fluorescence units). The normalized data were fitted to a linear model using the quality weight of each array (39). The differential expression was calculated using a moderated empirical Bayes *t* test (40). The resulting *P* values represented the false discovery rate (FDR) adjusted across the whole microarray data set for the normalization among multiple data sets (41). A threshold FDR of $<0.05$ was used to detect significant differential gene expression. We annotated the relevant target genes based on the genome information of Ensemble release 67 using the biomaRt package (42).

**Quantitative real-time RT-PCR.** $CD41^+$ cells were enriched from a culture of E13.5 fetal liver cells or adult bone marrow cells as described above. Total RNA was purified from sorted $CD41^+$ cells, and cDNA was synthesized using random hexamers. Real-time PCR was performed using an ABI7300 sequence detection system. The reaction was performed for 40 to 60 cycles of 30 s at 95°C and 1 min at 60°C using quantitative PCR (qPCR) MasterMix (Eurogenetec, Seraing, Belgium) or Power SYBR green PCR master mix (Applied Biosystems, Foster City, CA). The primers and probes used for the quantitative PCR are described in Table S1 in the supplemental material. rRNA control reagents (Applied Biosystems, Foster City, CA) were used as an internal control. The expression of each gene was normalized to the rRNA expression. The PCR assays were conducted in triplicate for each sample, and all experiments were repeated three times.

**ChIP, library preparation, and deep sequencing.** ChIP was performed using a day 3 primary culture of megakaryocytes from E13.5 fetal livers of wild-type mice with an anti-p45 antibody (16), as described previously (19, 23). Briefly, approximately $2 \times 10^6$ primary megakaryocytes were fixed with 1% formaldehyde for 10 min at room temperature. After neutralization with 125 mM glycine, the cells were washed in cold phosphate-buffered saline (PBS) twice and lysed in cell lysis buffer (5 mM PIPES-KCl, pH 8.0, 85 mM KCl, 0.5% NP-40, 1 mM phenylmethylsulfonyl fluoride [PMSF], 1× Complete [Roche, Basel, Switzerland]) for 10 min on ice. The chromatin was pelleted by centrifugation at 2,000 rpm for 5 min at 4°C, resuspended in nuclear lysis buffer (50 mM Tris-HCl, pH 8.0, 10 mM EDTA, 1% SDS, 1 mM PMSF, 1× Complete [Roche]), and sonicated on ice. Chromatin was incubated with the anti-p45 antibody and immunoabsorbed using a mixture of protein A plus protein G-Sepharose (GE Healthcare, Waukesha, WI). The input and ChIP DNA were used to generate sequencing libraries according to the manufacturer's instructions for the Illumina genome analyzer, with certain modifications. After PCR preamplification, size selection was performed by agarose gel electrophoresis, followed by the excision and purification of DNA fragments in the range of 400 bp. The purified libraries were sequenced on an Illumina 1G genome analyzer. Numbers of sequence reads for the pulled-down sample and input were 35,297,195 and 36,144,370, respectively.

**ChIP-Seq data analysis.** Sequences were mapped to mouse genomic sequences (mm9 according to the UCSC Genome Browser [http://genome.ucsc.edu/]) using the sequence alignment program Eland (43). To identify significant p45 binding regions in the ChIP-Seq data, we used MACS software (44) for peak calling. The default *P* value threshold of

**TABLE 1** Comparison of peak calling by MACS only and that by MACS and FindPeaks

| Parameter | Peak-calling result by: | |
|---|---|---|
| | MACS only | MACS and FindPeaks |
| Total no. of peaks | 1,922 | 1,390 |
| No. of genes to which p45 ChIP-Seq peaks are assigned | 1,794 | 1,306 |
| No. of peaks assigned to genes downregulated in *p45*-null megakaryocytes | 98 | 76 |
| No. of corresponding genes | 78 | 62 |
| No. of peaks assigned to genes upregulated in *p45*-null megakaryocytes | 25 | 20 |
| No. of corresponding genes | 22 | 17 |
| No. of peaks with NF-E2 motif and its related sequences | 1,224 | 888 |
| Frequency | 63.7% (1,244/1,922) | 63.9% (888/1,390) |
| No. of peaks with perfect NF-E2 motifs | 280 | 230 |
| Frequency | 14.6% (280/1,922) | 16.5% (230/1,390) |
| No. of genes containing p45 ChIP peaks with NF-E2 motif and its related sequences | 1,164 | 844 |
| Frequency | 64.9% (1,164/1,794) | 64.6% (844/1,306) |
| No. of downregulated genes in *p45*-null megakaryocytes containing peaks with NF-E2 motif and its related sequences | 60 | 49 |
| Frequency | 3.3% (60/1,794) | 3.7% (49/1,306) |
| No. of upregulated genes in *p45*-null megakaryocytes containing peaks with NF-E2 motif and its related sequences | 15 | 10 |
| Frequency | 0.84% (15/1,794) | 0.77% (10/1,306) |
| No. of genes not containing p45 ChIP peaks with NF-E2 motif or its related sequences | 630 | 462 |
| Frequency | 35.1% (630/1,794) | 35.4% (462/1,306) |
| No. of downregulated genes in *p45*-null megakaryocytes not containing peaks with NF-E2 motif or its related sequences | 18 | 13 |
| Frequency | 1.0% (18/1,794) | 1.0% (13/1,306) |
| No. of upregulated genes in *p45*-null megakaryocytes not containing peaks with NF-E2 motif or its related sequences | 7 | 7 |
| Frequency | 0.39% (7/1,794) | 0.54% (7/1,306) |

1.0E−5 was applied. The peaks obtained in this way were assigned to the genes using the ChIPpeakAnno package (45) of R Bioconductor. If a peak resided within a gene, the peak was assigned to the gene. If a peak was not within a gene, the peak was assigned to the gene whose transcription initiation site was the closest. We also used FindPeaks 4.0 software (46) for peak detection and compared the results to those obtained from MACS (Table 1). To ascribe the relationship between peaks and specific genes (see Tables S2 and S3 in the supplemental material), peaks detected by both programs were identified and assigned to genes by following the rules described above.

**Motif analysis.** Multiple Em for Motif Elicitation (MEME) was used to identify statistically overrepresented consensus motifs within the range spanning from 200 bp upstream of peak starts to 200 bp downstream of peak ends. The peak sequences were masked using RepeatMasker (http://repeatmasker.org) to prevent the detection of repeat sequences. Peaks with mask ratios of less than 60% were used for the motif analysis. For re-searching the motif sequences obtained from MEME and their related sequences, we defined GC TGA G/C TCA T/C as a complete NF-E2 motif and GC XXX G/C TCA as an NF-E2 motif-related sequence.

**ChIP assays.** ChIP assays were performed as described previously (19, 23), using a day 3 primary culture of megakaryocytes from E13.5 fetal livers of wild-type mice. The immunoprecipitation was conducted with control rabbit IgG or rabbit serum, anti-p45 (16), and anti-MafG (22) antibodies. The PCR was performed in triplicate using qPCR MasterMix (Eurogenetec, Seraing, Belgium) or Power SYBR green PCR master mix (Applied Biosystems, Foster City, CA) with ChIP or input DNA. The ChIP enrichment relative to input DNA was calculated from the quantitative real-time PCR results as fold enrichment. The primers used in the ChIP assay are described in Table S1 in the supplemental material. The PCR assays were conducted in triplicate for each sample, and all of the experiments were repeated three times.

**Hematological analysis and bleeding time.** Peripheral blood was collected from individual 8- to 10-week-old mice. The hematopoietic indices were measured using an automatic blood cell analyzer (Nihon Koden, Tokyo, Japan). Bone marrow megakaryocytes were enriched as described previously (24). Briefly, bone marrow cells were collected from the femurs and tibias of 8- to 10-week-old mice. The bone marrow samples were flushed with 5 ml CATCH medium (Hanks' balanced salt solution, 1 mM adenosine, 2 mM theophylline, and 0.38% sodium citrate at pH 7.2) into a plastic dish. To enrich for megakaryocytes, the marrow cells were centrifuged in 50% Percoll–CATCH solution (density, 1.065 g/ml) at 1,100 rpm at 20°C for 30 min. The cells in the intermediate layer were recovered and cytospun using a Shandon Cytospin 4 instrument (Thermo, Waltham, MA). The cytospun samples were stained with Wright-Giemsa and also reacted with an fluorescein isothiocyanate (FITC)-conjugated anti-CD41 antibody (clone MWReg30; BD Biosciences Pharmingen, Franklin Lakes, NJ). 4′,6-Diamidino-2-phenylindole (DAPI) was used for the nuclear counterstaining. The bleeding-time assay was conducted by excising the tip of the tail (5 mm from the tip). The tail was blotted with filter paper every 15 s until the paper was no longer bloodstained. The bleeding was manually stopped at 1,200 s after cutting the tail.

**Flow-cytometric analysis of megakaryocytes.** Whole bone marrow cells were collected from the femurs and tibias of 8- to 10-week-old mice and stained with phycoerythrin (PE)-conjugated anti-CD41 (clone MWReg30; BD Biosciences Pharmingen) and FITC-conjugated anti-CD61 (clone 2C9.GCBD; Biosciences Pharmingen) antibodies for 30 min on ice. The samples were washed with PBS and analyzed using flow cytometry (Calibur; BD, Franklin Lakes, NJ).

**FCA of platelets.** Flow cytometry-based platelet aggregation assay (FCA) was performed as described previously (47). In brief, whole blood was collected from 8- to 10-week-old mice in a heparinized tube (MTSC-LIHEP; Kent Scientific Corp) using a heparinized glass needle. One aliquot of whole blood was incubated with a PE-conjugated anti-CD9 antibody (clone eBioKMC8; eBioscience), and the other was incubated with an antigen-presenting cell (APC)-conjugated anti-CD9 antibody (clone eBioKMC8; eBioscience) for 20 min. Subsequently, 1 ml of Sequestrine

buffer (17.5 mM $Na_2HPO_4$, 8.9 mM $Na_2EDTA$, 154 mM NaCl [pH 6.9], and 0.1% [wt/vol] bovine serum albumin) was added to each sample. After centrifugation at 2,250 × *g* for 5 min, the supernatant was discarded. Each pellet was resuspended in 250 μl HEPES medium with glucose (132 mM NaCl, 6 mM KCl, 1 mM $MgSO_4$, 1.2 mM $KH_2PO_4$, 20 mM HEPES [pH 7.4], and 5 mM glucose) supplemented with 10% citrate pool plasma (Kohjin Bio, Saitama, Japan). The single-stained cells were mixed, stimulated with 0 to 2.0 U/ml thrombin for 5 min at 37°C, fixed in a 400× volume of 0.5% formaldehyde in PBS, and analyzed using flow cytometry. Platelet activation in response to thrombin was examined using flow cytometry with an anti-CD62P antibody. Whole blood at a 1:400 dilution was incubated with PE-conjugated anti-CD41 (clone MWReg30; BD Biosciences Pharmingen) and FITC-conjugated anti-CD62P (RB40.34; BD Biosciences Pharmingen) antibodies and stimulated with 0 to 2.0 U/ml thrombin for 20 min at room temperature. The thrombin stimulation was ended by a further 10-fold dilution with PBS, and the sample was analyzed using flow cytometry.

**Microarray data accession number.** Microarray data for WT and $p45^{-/-}$ megakaryocytes are available in GEO under accession no. GSE35645.

## RESULTS

**Genome-wide p45 chromatin occupancy in megakaryocytes.** To establish a framework for understanding p45 function in megakaryopoiesis, we used ChIP-Seq to define p45 chromatin occupancy sites in megakaryocytes. We used an anti-p45 antibody to analyze endogenous p45 chromatin occupancy in primary cultured megakaryocytes (Fig. 1A). Analysis of the immunoprecipitated DNA by MACS revealed 1,922 peaks which represent candidate p45 occupancy sites in megakaryocytes. Assignment of each occupancy site to the closest gene revealed 1,794 genes. These data were validated by quantitating p45 occupancy at 43 representative peaks using a real-time PCR-based analysis (Fig. 1B). The third intron of *Txs* (*Txs* intron 3) and the *Cd9* promoter region were used as negative-control loci. The enrichment was significantly higher at 39 out of 43 loci than at *Txs* intron 3, validating the ChIP-Seq assay. The p45 occupancy sites were located relatively near the transcription start sites (TSS), especially in regions extending from the TSS to 5 kbp downstream of the TSS (Fig. 1C). However, classification of the genome into three regions, promoters (5 kbp upstream and 5 kbp downstream of TSS), transcribed regions outside promoters, and intergenic regions, revealed a widespread distribution of the p45 binding sites (Fig. 1D). According to a recent analysis using the ENCODE database, NF-E2 is categorized as a remote element preferential transcription factor (48), consistent with our analysis of primary megakaryocytes.

We used MEME to interrogate the specific DNA sequence composition of p45 occupancy sites. This analysis revealed a typical NF-E2 motif, A/G TGA C/G TCA GC (GC TGA G/C TCA T/C in the complementary strand), which was significantly (E value, 9.7e-199) overrepresented at the occupancy sites (Fig. 1E). All other motifs frequently obtained from MEME were repetitive sequences (data not shown). We reanalyzed the p45 occupancy sites to test for the presence of the NF-E2 motif (A/G TGA C/G TCA GC and GC TGA G/C TCA T/C) and related sequences (TGA C/G nnn GC and GC nnn G/C TCA). These motifs were identified in 63.7% of the total p45 ChIP-Seq peaks (1,224 out of 1,922 peaks), and 280 peaks (14.6% of the total number of peaks) contained perfect NF-E2 binding motifs.

Since the AP-1 binding site (TGA G TCA) resembles the NF-E2 motif, we examined the presence of AP-1 motifs within the p45 ChIP-Seq peaks. The complete AP-1 motif resided in 533 peaks (27.7% of the total peaks). Among them, 262 peaks harbored AP-1 motifs without any flanking GC dinucleotides (canonical AP-1 motifs); p45-small Maf heterodimers do not bind canonical AP-1 motifs with high affinity, since the flanking GC is essential for DNA recognition by small Maf proteins (20). However, most of these peaks also contained NF-E2 motif-related sequences in parallel. The number of peaks exclusively containing canonical AP-1 motifs was 72, which accounted for 3.7% of the total number of p45 ChIP-Seq peaks. This result indicated that the canonical AP-1 motif is a minor motif present at p45 occupancy sites, supporting the concept that small Maf is a frequent heterodimeric partner of p45.

To identify target genes that are directly activated by p45 in megakaryocytes, we conducted microarray analysis to compare the transcriptomes of WT and $p45^{-/-}$ megakaryocytes (GEO accession number GSE35645) (Fig. 1A). This analysis revealed 443 and 324 genes with expression levels significantly lower and higher, respectively, in $p45^{-/-}$ than in wild-type cells (Fig. 1F). Seventy-eight downregulated genes were occupied by p45; therefore, they were candidates for direct p45-activated target genes. p45 occupied 22 upregulated genes, which were candidates for direct p45-repressed target genes. The peak numbers assigned to the activated and repressed p45 target genes were 98 and 25, respectively.

**Direct p45 target gene candidates in megakaryocytes include important regulators of platelet function.** Since the NF-E2 motif was the sole *cis*-regulatory element overrepresented in the p45 ChIP-Seq data, we focused on genes containing p45 ChIP-Seq peaks with an accompanying NF-E2 motif and its related sequences. To reduce false positives, we reanalyzed the sequence data using two different peak-calling programs, MACS and FindPeaks, which revealed 1,390 peaks detected by both programs (Table 1). A total of 888 of the 1,390 peaks contained the NF-E2 motif and its related sequences, which correspond to 844 genes. Among the 888 peaks, 61 and 11 peaks were assigned to 49 and 10 genes that were downregulated and upregulated in $p45^{-/-}$ megakaryocytes, respectively (Fig. 2A; also see Table S2 in the supplemental material). These genes represent candidates for direct NF-E2 activation and NF-E2 repression. We functionally annotated these genes with DAVID (49) and GREAT (50). Genes relating to phosphatase activity and vesicle formation were enriched in the NF-E2-activated genes, but no significant functional enrichments were apparent for the NF-E2-repressed genes (see Table S3). Importantly, 15 of the 49 genes encoded proteins involved in platelet function (platelet genes) (Fig. 2A; also see Table S2).

Of the 15 candidates for direct NF-E2 activation, we selected 8 genes whose ChIP-Seq peaks had lower *P* values with more statistical significance and tested whether their expression is p45 regulated. For this purpose, we utilized $p45^{-/-}$:p45-Tg mice, which express p45 specifically in the erythromegakaryocytic lineage under the regulation of transcriptional elements from the *Gata1* locus (hematopoietic regulatory domain, or *G1HRD*) in the *p45*-null background. This mouse strain exhibits a normal platelet count (17) (Table 2). Expression of *Selectin P* (*Selp*), *Solute carrier family 6, member 4* (*Slc6a4*), and *Myosin, light polypeptide 9* (*Myl9*) was decreased in *p45*-null megakaryocytes and restored in $p45^{-/-}$:p45-Tg megakaryocytes, correlating with p45 activity. In contrast, a reproducible p45 dependency was not apparent for the remaining five genes, *Solute carrier family 2, member 3* (*Slc2a3*), *Low density lipoprotein receptor-related protein 8* (*Lrp8*), *FYN binding protein* (*Fyn*), *Secretory*

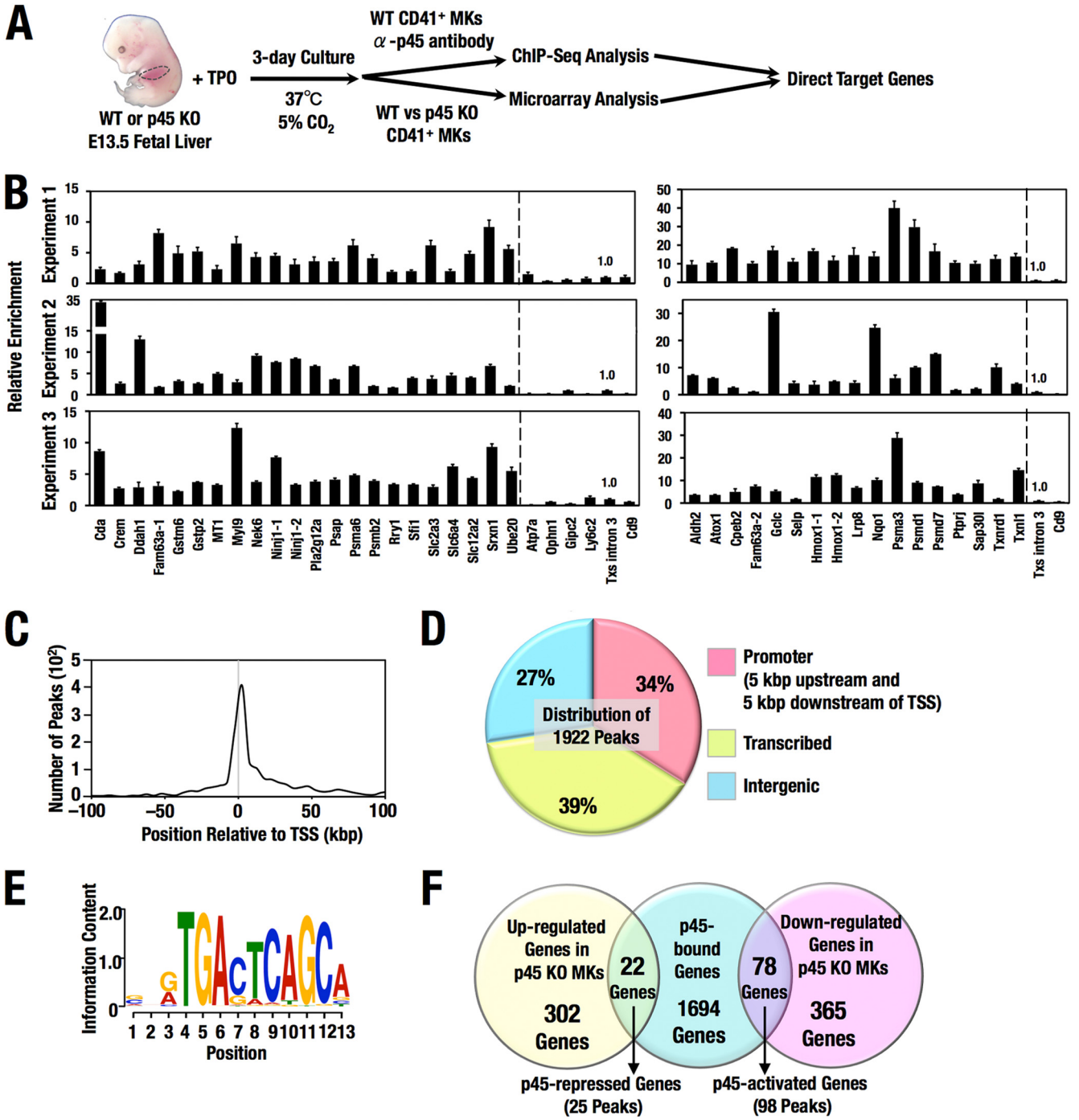


**FIG 1** Genome-wide analysis of p45 chromatin occupancy. (A) Primary megakaryocytes (MKs) cultured from fetal livers were used for ChIP-Seq analysis and microarray analysis. The former was performed with an anti-p45 antibody using wild-type (WT) MKs, and the latter was performed using MKs from both WT and *p45*-null (p45 KO) mice. (B) Validation of the ChIP-Seq results using ChIP-PCR analysis. A total of 43 ChIP-Seq hits were selected, and two indifferent loci, the third intron of the *Txs* gene (*Txs* intron 3) and the promoter region of the *Cd9* gene (Cd9), were used as negative controls. The enrichment of each locus relative to the input is shown after setting the enrichment of *Txs* intron 3 to 1. The ChIP-Seq hits whose relative enrichments are below or above 10 in experiment 1 are shown in the left and right panels, respectively. Results from three independent experiments are shown. The average values and standard deviations (SDs) were calculated from technical triplicate samples. (C) The distribution of p45 ChIP-Seq peaks relative to the transcription start sites of the closest genes. (D) A pie diagram showing the distribution of p45-occupied ChIP-Seq peaks. The peak positions were classified into 3 regions, the promoter (5 kbp upstream and 5 kbp downstream of the TSS), transcribed region (gene body region that is not included in the promoter), and intergenic region. (E) A sequence logo of an overrepresented motif from the p45-occupied ChIP-Seq peaks. (F) A Venn diagram representation of the association between the p45-bound genes (1,794 genes) and the genes downregulated and upregulated in p45 KO MKs compared to WT MKs (443 and 324 genes, respectively). Seventy-eight genes, to which 98 peaks were assigned, were both bound by p45 and decreased in p45 KO MKs and were identified as p45-activated genes. Twenty-two genes, to which 25 peaks were assigned, were both bound by p45 and increased in p45 KO MKs and were identified as p45-repressed genes.

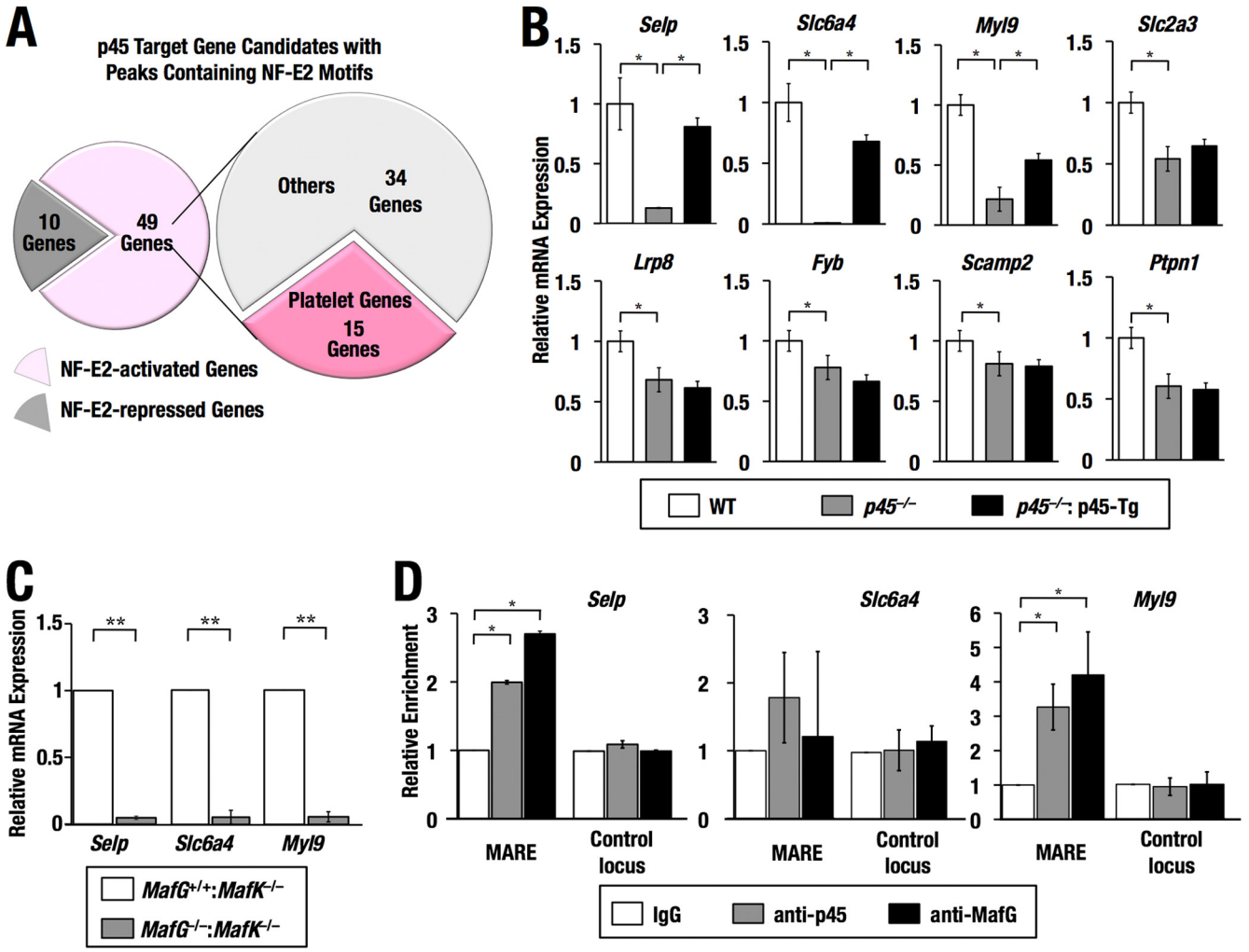


**FIG 2** Identification of platelet genes that are directly regulated by NF-E2. (A) Pie diagrams showing p45 target genes with peaks containing NF-E2 motifs. Among 844 genes with peaks containing NF-E2 motifs, 49 and 10 genes were repressed and activated, respectively, in *p45*-null megakaryocytes. The former 49 genes represent candidates for direct NF-E2 activation, among which 15 are involved in platelet function (platelet genes). The latter 10 genes are regarded as candidates of NF-E2-repressed genes. (B) The expression levels of representative platelet genes in primary cultured megakaryocytes from WT, $p45^{-/-}$, and $p45^{-/-}$:p45-Tg fetal livers. The average values and SDs were calculated from three independent experiments. The average values for the WT were set to 1. Student's *t* test was used to calculate statistical significance. *, $P < 0.05$. (C) Expression levels of the three platelet genes in primary cultured megakaryocytes from $MafG^{+/+}$:$MafK^{-/-}$ and $MafG^{-/-}$:$MafK^{-/-}$ fetal livers. The expression levels for $MafG^{+/+}$:$MafK^{-/-}$ megakaryocytes were set to 1. The averages and SDs of relative expression for $MafG^{-/-}$:$MafK^{-/-}$ megakaryocytes were calculated from three independent experiments. Welch's *t* test was used to calculate statistical significance. **, $P < 0.01$. (D) The relative enrichment of the p45-ChIP peak regions assigned to the three platelet genes. ChIP analysis was conducted with primary megakaryocytes derived from WT fetal livers using antibodies against p45 and MafG. Rabbit IgG or rabbit serum was used for the negative control. A randomly selected region surrounding each p45-ChIP peak was used for the control locus. The enrichment relative to the input of IgG was set to 1. The averages and SDs of relative enrichment for anti-p45 and anti-MafG antibodies were calculated from three independent experiments. Welch's *t* test was used to calculate the statistical significance. *, $P < 0.05$.

*carrier membrane protein 2* (*Scamp2*), and *Protein tyrosine phosphatase, nonreceptor type 1* (*Ptpn1*) (Fig. 2B).

We tested the contribution of small Maf to the regulation of the three platelet genes that are deemed direct NF-E2-activated genes. Among three small Maf proteins, MafG and MafK are major heterodimeric partners of p45, since $MafG^{-/-}$:$MafK^{-/-}$ mice displayed severe thrombocytopenia and bleeding propensity comparable to that observed in $p45^{-/-}$ mice (24). MafG appears to be the principle partner, since $MafG^{-/-}$ mice display mild thrombocytopenia, but $MafK^{-/-}$ mice do not exhibit this phenotype (32). Accordingly, we examined the contribution of MafG by comparing primary megakaryocytes cultured from $MafG^{+/+}$:$MafK^{-/-}$ and $MafG^{-/-}$:$MafK^{-/-}$ fetal livers. All three genes, *Selp*, *Slc6a4*, and *Myl9*, were significantly downregulated in $MafG^{-/-}$:$MafK^{-/-}$ megakaryocytes versus $MafG^{+/+}$:$MafK^{-/-}$ megakaryocytes (Fig. 2C).

We conducted ChIP analysis with anti-p45 and anti-MafG antibodies using primary wild-type megakaryocytes. Both p45 and MafG were enriched significantly at MARE-containing p45 occupancy sites assigned to *Selp* and *Myl9*, while no enrichment was observed at a control locus that was arbitrarily selected from the genomic region surrounding each p45 occupancy site (Fig. 2D). Only marginal enrichment for both antibodies was apparent at the *Slc6a4* peak. These results indi-

**TABLE 2** Blood counts of compound mutant mice in *p45*-null background

| Mouse line[a] (*n*) | Blood count result[b] | | | |
|---|---|---|---|---|
| | No. of RBC ($\times 10^4/\mu l$) | Hb (g/dl) | Hct (%) | No. of Plt ($\times 10^4/\mu l$) |
| WT (5) | 982 ± 19 | 15.5 ± 1.6 | 46.2 ± 3.5 | 90.9 ± 4.9 |
| $p45^{-/-}$:Tg 207 (6) | 953 ± 52 | 14.5 ± 0.5 | 46.3 ± 1.1 | 69.9 ± 8.6 |
| WT (10) | 944 ± 73 | 14.4 ± 1.6 | 44.1 ± 4.1 | 97.6 ± 12.8 |
| $p45^{-/-}$:ΔNTD Tg 311 (10) | 967 ± 52 | 14.2 ± 1.3 | 43.5 ± 3.1 | 27.6 ± 8.7 |
| $p45^{-/-}$:ΔNTD Tg 340 (13) | 961 ± 76 | 13.3 ± 1.3 | 41.7 ± 2.9 | 27.0 ± 13.4 |

[a] Wild-type and $p45^{-/-}$:Tg 207 mice from the same breeding colony were examined at 2 months of age. Wild-type and $p45^{-/-}$:ΔNTD Tg 311 and 340 mice from the same breeding colony were examined at 2 months of age.
[b] The values are expressed as means ± standard deviations. RBC, red blood cells; HB, hemoglobin; Hct, hematocrit; Plt, platelet.

cate that the platelet genes *Selp* and *Myl9* are directly activated by p45 in megakaryocytes.

**p45 N terminus requirement for platelet gene expression.** Myosin light chain 2, encoded by *Myl9*, is important for proplatelet formation (51), a major process of platelet production regulated by p45 in megakaryocytes (26). In contrast, P-selectin, encoded by *Selp*, is a cell adhesion molecule that is exposed on the surface of stimulated platelets mediating platelet-leukocyte binding (52, 53), and it exerts a critical role in thrombogenesis (54). These results suggested that p45 contributes to both platelet production and function. Since most $p45^{-/-}$ mice die before weaning due to severe thrombocytopenia, and since very few platelets are detected in the peripheral blood of $p45^{-/-}$ mice, even if they survive to adulthood, an alternative model to $p45^{-/-}$ mice was necessary to dissect how p45 controls platelet function.

p45 can be structurally divided into two parts: the N-terminal half, which mediates transactivation, and the C-terminal half, which mediates heterodimerization and DNA binding (55). The N-terminal 38 amino acids are important for p45 transactivation activity. A p45 mutant lacking these 38 amino acids (ΔNTD) exhibits significantly reduced transactivation capacity (16, 17). We previously reported $p45^{-/-}$:ΔNTD-Tg mice, which express ΔNTD driven by *G1HRD* in a *p45*-null background (17). $p45^{-/-}$:ΔNTD-Tg mice display only mild thrombocytopenia and survive to adulthood (Table 2). We utilized line 311 of $p45^{-/-}$:ΔNTD Tg mice for subsequent analyses.

We evaluated megakaryocyte differentiation in $p45^{-/-}$:ΔNTD-Tg mice. The percentage of $CD41^+$ $CD61^+$ double-positive megakaryocytes in whole bone marrow cells was lower in $p45^{-/-}$:ΔNTD-Tg mice than in wild-type and $p45^{-/-}$:p45-Tg mice (Fig. 3A). However, Wright-Giemsa staining of the cytospun samples demonstrated that the megakaryocytes in the $p45^{-/-}$:ΔNTD-Tg mice were as mature as those of wild-type and $p45^{-/-}$:p45-Tg mice (Fig. 3B, upper). Immunofluorescence with anti-CD41 antibody showed almost comparable or slightly larger megakaryocytes in $p45^{-/-}$:ΔNTD-Tg mice than in control mice, validating that megakaryocytic differentiation was not impaired in $p45^{-/-}$:ΔNTD-Tg mice (Fig. 3B, lower). We quantitated the expression levels of three platelet genes in primary megakaryocytes derived from $p45^{-/-}$:ΔNTD-Tg fetal liver cells. Expression of the platelet genes was significantly reduced in the $p45^{-/-}$:ΔNTD-Tg megakaryocytes (Fig. 3C). Therefore, the N-terminal region of p45 is required for platelet gene expression.

***p45*$^{-/-}$:ΔNTD-Tg mice display platelet hypofunction.** Based on the observation that p45-regulated platelet genes were downregulated in $p45^{-/-}$:ΔNTD-Tg megakaryocytes, we evaluated the platelet hemostatic function of $p45^{-/-}$:ΔNTD-Tg mice. Although $p45^{-/-}$:ΔNTD-Tg mice showed no evidence of spontaneous hemorrhage over the first 8 weeks of life in a controlled environment, their mean bleeding time was significantly longer than that of control mice (wild type and $p45^{+/-}$), whereas no difference was observed between control mice and $p45^{-/-}$:p45-Tg mice (Fig. 4A). Two of five $p45^{-/-}$:ΔNTD-Tg mice did not reach hemostasis within 20 min. This hemostatic defect appeared to be disproportionate to the circulating platelet count, which was reduced to approximately 30% of the normal level (Table 2), suggesting platelet dysfunction in $p45^{-/-}$:ΔNTD-Tg mice.

To test this possibility, we quantitated thrombin-induced platelet aggregation using a flow-cytometric platelet aggregation assay (47). One aliquot of whole blood reacted with a PE-conjugated anti-CD9 antibody and another reacted with an APC-conjugated anti-CD9 antibody were mixed and stimulated with thrombin (Fig. 4B, upper). After stimulation, platelet aggregates fall in the double-positive quadrant, and the single-positive platelet populations decrease as the platelet aggregation proceeds. We plotted the percentage of single-positive platelet populations (Q1 + Q4) and observed that the expected decrease was delayed in $p45^{-/-}$:ΔNTD-Tg mice versus wild-type mice but not in $p45^{-/-}$:p45-Tg mice (Fig. 4B, lower). This result indicates that thrombin-dependent platelet aggregation is impaired in $p45^{-/-}$:ΔNTD-Tg mice.

To examine platelet function at the single-cell level, we measured the exposure of P-selectin on the surface of platelets in response to thrombin. With increasing concentrations of thrombin, the P-selectin-positive population increased incrementally for both wild-type and $p45^{-/-}$:ΔNTD-Tg platelets. However, the positive percentage was significantly lower in the latter than in the former (Fig. 4C, lower right). The peak intensity of the P-selectin signals was also lower in $p45^{-/-}$:ΔNTD-Tg platelets (Fig. 4C, lower left). These results were explained by the reduced protein level of P-selectin resulting from the decreased expression of the *Selp* gene (encoding CD62P/P-selectin) in $p45^{-/-}$:ΔNTD-Tg megakaryocytes. The response of $p45^{-/-}$:p45-Tg platelets to thrombin was comparable to that of wild-type platelets (Fig. 4C, upper), consistent with the comparable expression of *Selp* in wild-type and $p45^{-/-}$:p45-Tg megakaryocytes (Fig. 2B). Thus, platelet function is compromised in $p45^{-/-}$:ΔNTD-Tg mice, suggesting that impaired p45 activity in megakaryocytes results in platelet hypofunction.

**Lung metastasis is inhibited in *p45*$^{-/-}$:ΔNTD-Tg mice.** It has been reported that platelet activation, especially P-selectin exposed on the surface of activated platelets, plays a key role in cancer metastasis (56–58). We tested whether the platelet hypofunction of $p45^{-/-}$:ΔNTD-Tg mice affected cancer metastasis. We utilized a well-established mouse model for cancer metastasis in which B16-F10 melanoma cells are intravenously injected and lung metastasis is scored by quantitating metastatic nodules detected on the lung surface. B16-F10 cells expressing tdTomato fluorescent protein (33) were used in this experiment.

The melanoma cells were injected into tail veins of $p45^{+/+}$, $p45^{-/-}$, and $p45^{-/-}$:p45-Tg mice obtained from the same breed-

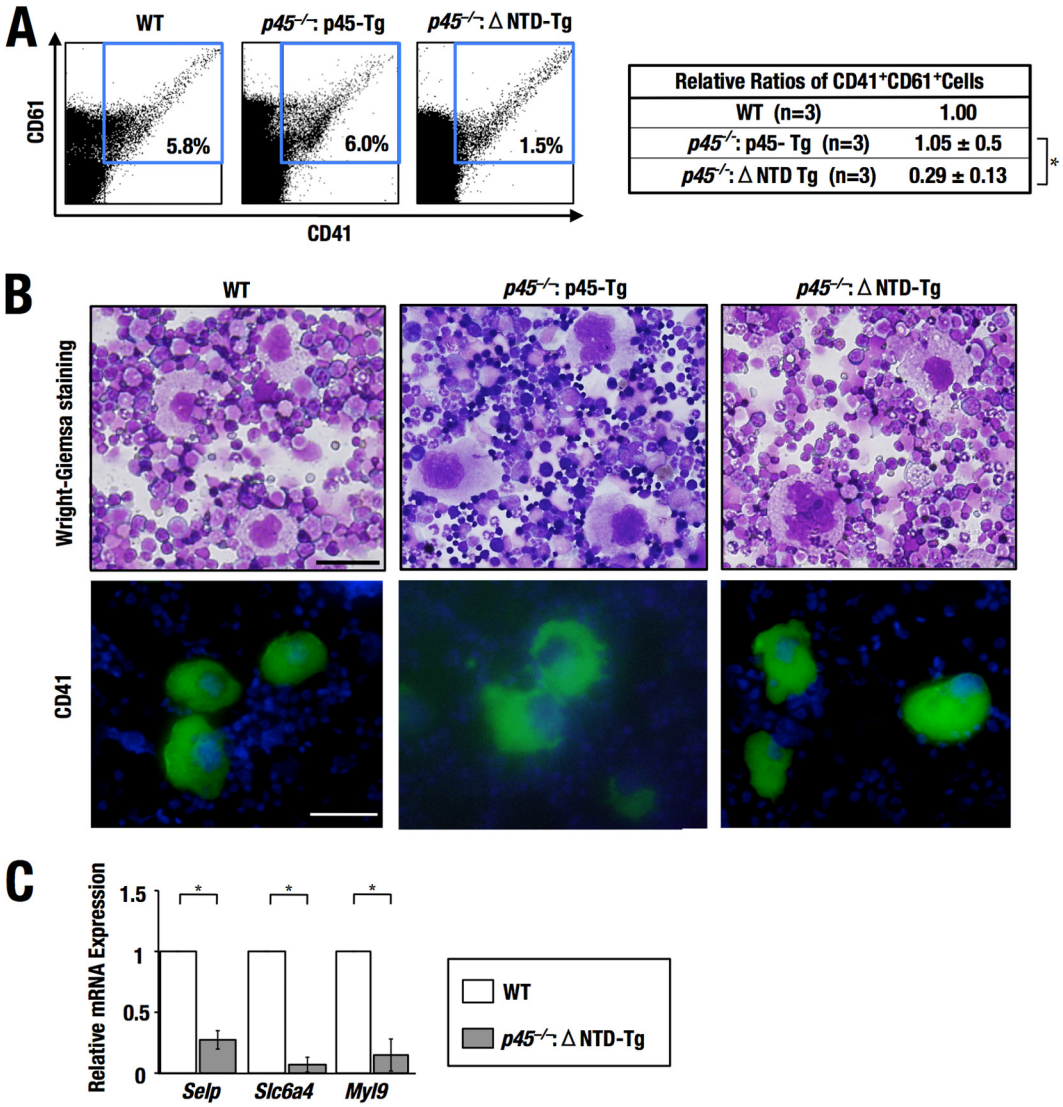


**FIG 3** Analysis of megakaryocytes in $p45^{-/-}$:ΔNTD-Tg mice. (A) CD41 and CD61 expression in the bone marrow cells of WT, $p45^{-/-}$:p45-Tg, and $p45^{-/-}$:ΔNTD-Tg mice (left). The representative frequencies of the $CD41^+$ $CD61^+$ double-positive megakaryocyte population (gates shown in blue) are indicated. The frequency of $CD41^+$ $CD61^+$ double-positive cells in WT bone marrow was set to 1. The averages and SDs of the relative frequency of the $CD41^+$ $CD61^+$ double-positive population were calculated for each genotype (WT, $n = 3$; $p45^{-/-}$:p45-Tg, $n = 3$; $p45^{-/-}$:ΔNTD-Tg, $n = 3$) (right). Student's $t$ test was used to calculate the statistical significance. *, $P < 0.05$. (B) Wright-Giemsa staining (upper) and immunofluorescence with an anti-CD41 antibody (lower) of cytospun preparations of bone marrow megakaryocytes from WT, $p45^{-/-}$:p45-Tg, and $p45^{-/-}$:ΔNTD-Tg mice. CD41, green; DAPI, blue. Scale bars correspond to 100 μm. (C) Expression levels of the three platelet genes in primary cultured megakaryocytes from WT and $p45^{-/-}$:ΔNTD-Tg fetal livers. The values for WT megakaryocytes were set to 1. The averages and SDs of relative expression for $p45^{-/-}$:ΔNTD-Tg megakaryocytes were calculated from three independent experiments. Welch's $t$ test was used to calculate statistical significance. *, $P < 0.05$.

ing colonies in the B6 background. Eighteen days after cell inoculation, numerous black nodules were observed in the wild-type lung, whereas no metastatic nodules were macroscopically detected in *p45*-null lung (Fig. 5A). The number of metastatic nodules in $p45^{-/-}$:p45-Tg lung was comparable to that in wild-type lung (Fig. 5B, left). This result suggests that expressing p45 in *p45*-null megakaryocytes using the *G1HRD* system promotes lung metastasis. Furthermore, the inhibition of lung metastasis in *p45*-null mice appears to be related to defective platelet production.

We then injected the melanoma cells into tail veins of $p45^{+/+}$, $p45^{-/-}$, and $p45^{-/-}$:ΔNTD-Tg mice obtained from the same breeding colonies in the B6 background. Significantly fewer nodules were apparent in lungs of $p45^{-/-}$:ΔNTD-Tg versus wild-type mice after 18 days of cell inoculation (Fig. 5A and B, right). This result provides evidence that an additional important platelet function is impaired in $p45^{-/-}$:ΔNTD-Tg mice, supporting the notion that p45 activity is important for conferring normal platelet function.

## DISCUSSION

Our genomic strategy identified 49 genes as candidates for direct activation by NF-E2 in megakaryocytes. Fifteen of these genes are known to have roles in platelet function. Utilizing multiple approaches, *Selp* and *Myl9* were verified as NF-E2-activated platelet

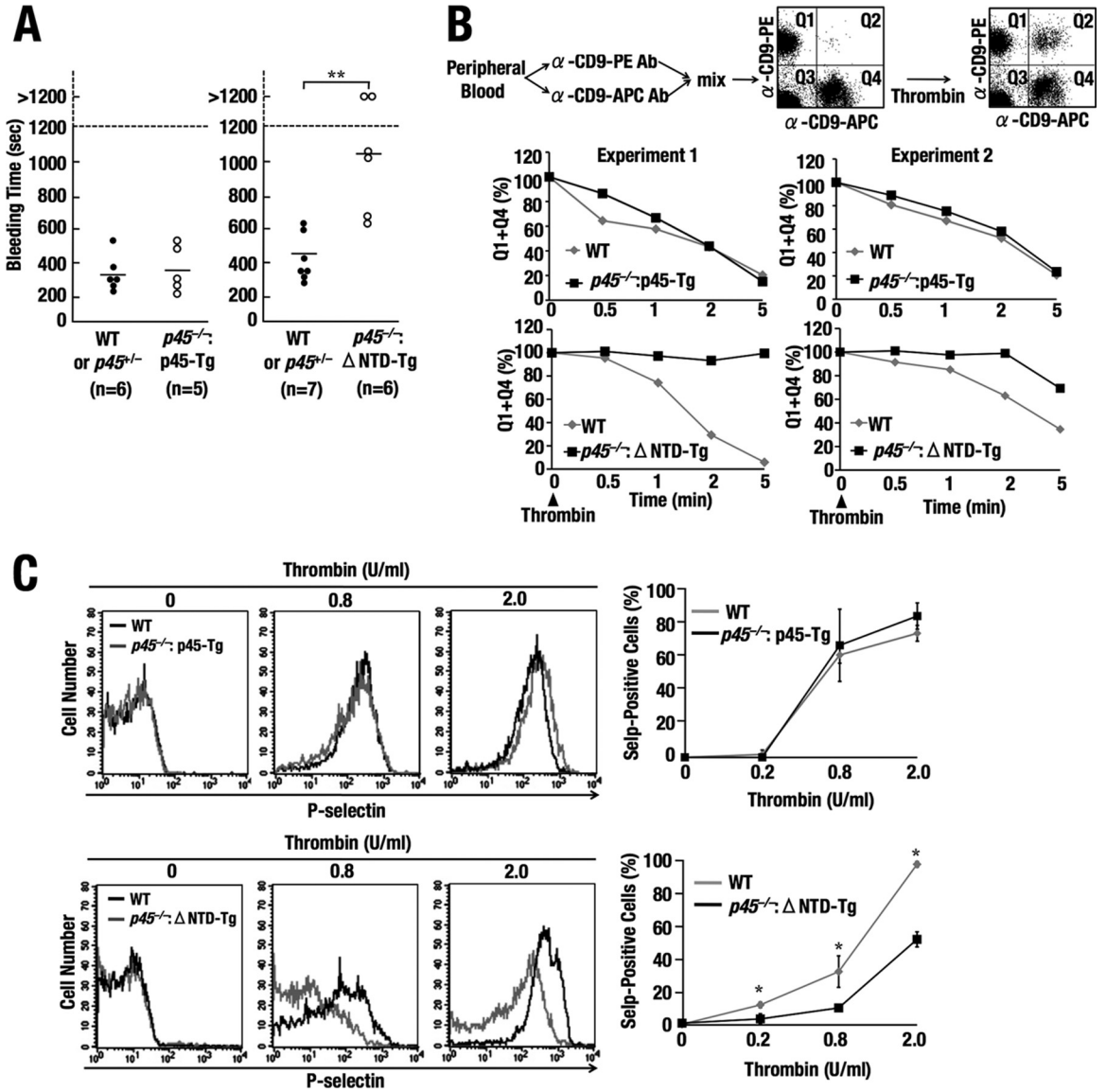


**FIG 4** N terminus of p45 confers normal platelet function. (A) The bleeding times of $p45^{-/-}$:p45-Tg mice and $p45^{-/-}$:ΔNTD-Tg mice compared to those of control mice (WT and $p45^{+/-}$ mice). A bleeding time longer than 1,200 s was deemed to be 1,200 s in the statistical calculation. The average values are indicated by bars. Student's *t* test was used to calculate the statistical significance. **, $P < 0.01$. (B) The analysis of thrombin-induced platelet aggregation by flow cytometry. A summary of the experimental procedure is illustrated (upper). One aliquot of whole blood reacted with a PE-conjugated anti-CD9 antibody and another reacted with an APC-conjugated anti-CD9 antibody were mixed and analyzed using flow cytometry before and after thrombin stimulation. The combined frequencies of the Q1 and Q4 particles are plotted (lower). The Q1+Q4 frequencies of $p45^{-/-}$:p45-Tg mice and $p45^{-/-}$:ΔNTD-Tg mice were compared to those of the WT mice. The results from two independent experiments are shown. (C) The analysis of thrombin-induced platelet activation by flow cytometry. Peripheral blood at a 1:400 dilution from WT, $p45^{-/-}$:p45-Tg, and $p45^{-/-}$:ΔNTD-Tg mice was stimulated with thrombin and reacted with an FITC-conjugated anti-CD62P antibody (left). The frequencies of platelets with fluorescence intensity above $10^2$ are plotted (right). Student's *t* test was used to calculate the statistical significance. *, $P < 0.05$.

genes. Mice expressing the N-terminal deletion mutant of p45, whose transcriptional activity is impaired, displayed decreased expression of platelet genes in megakaryocytes and platelet hypofunction, accompanied by mild thrombocytopenia. Interestingly, the murine model of cancer metastasis revealed impaired function of platelets produced from megakaryocytes expressing the mutant p45, since essentially no metastasis was apparent in lungs from $p45^{-/-}$:ΔNTD-Tg mice. These results supported a model in which p45 is an important determinant of platelet function in addition to promoting the production of platelets.

Among the 844 genes possessing p45 ChIP-Seq peaks containing the NF-E2 motif-related sequences, 49 and 10 genes were deemed NF-E2-activated and NF-E2-repressed genes, respectively. p45 is conventionally considered to be a transcriptional activator based on structure-function analyses (16, 17, 59). This is consistent with our results in which the expression of 49 genes decreased in the absence of p45. As p45 contributes to the recruitment of the methyltransferase G9a to the β-globin locus, and as this is implicated in repression of the embryonic globin gene (60), in principle, p45 might utilize a similar mechanism for repressing the 10 genes.

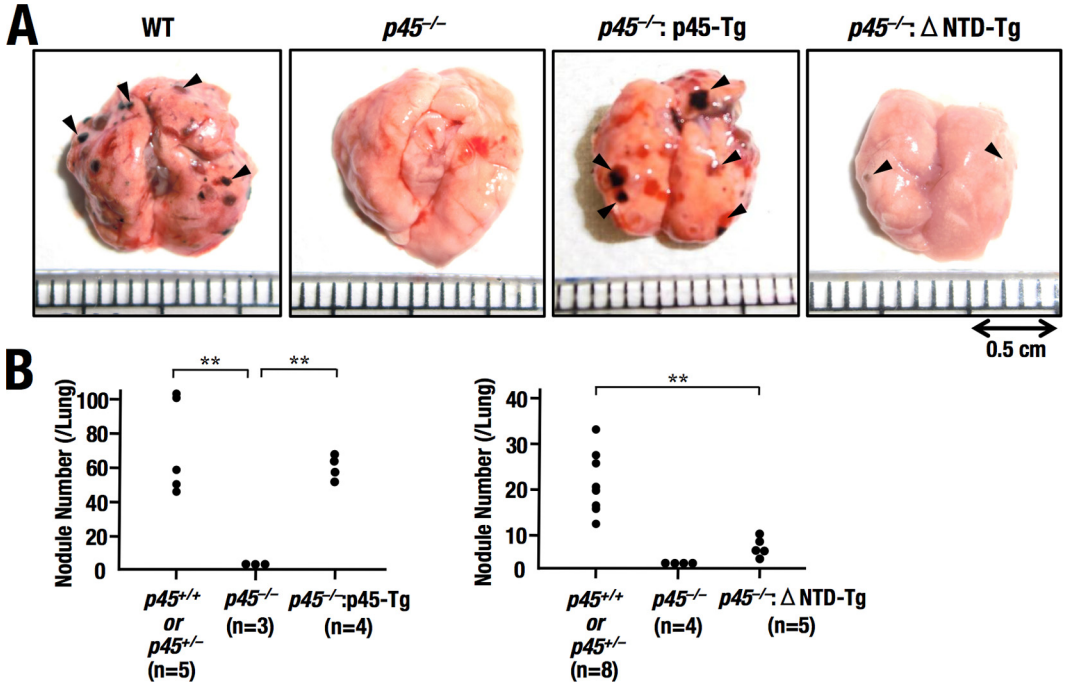


**FIG 5** N terminus of p45 promotes lung metastasis. (A) Example of tumor burden in lungs from WT, $p45^{-/-}$, $p45^{-/-}$:p45-Tg, and $p45^{-/-}$:ΔNTD-Tg mice. Arrowheads indicate metastatic nodules. (B) The number of metastatic nodules per lung ($p45^{+/+}$ or $p45^{+/-}$, $n = 5$; $p45^{-/-}$, $n = 3$; $p45^{-/-}$:p45-Tg, $n = 4$ [left]; $p45^{+/+}$ or $p45^{+/-}$, $n = 8$; $p45^{-/-}$, $n = 4$; $p45^{-/-}$:ΔNTD-Tg, $n = 5$ [right]). Macroscopically detectable nodules were counted. Student's *t* test was used to calculate the statistical significance. **, $P < 0.01$.

Expression levels of the remaining 785 genes did not differ significantly between *p45*-null and wild-type megakaryocytes (see Table S2 in the supplemental material). In principle, one interpretation of these results is that p45 occupancy at the 785 genes does not contribute to transcription. Alternatively, Nrf2 and other CNC proteins may compensate for the loss of p45 function at some of these loci in *p45*-null megakaryocytes. Previously, we demonstrated that p45 and Nrf2 coregulate cytoprotective genes, which are typical Nrf2 target genes, in megakaryocytes (61). The expression levels of these genes do not decrease in *p45*-null megakaryocytes. A double deletion of p45 and Nrf2 is required to reduce the expression of these genes. In the current study, p45 ChIP-Seq peaks containing NF-E2 motifs resided at Nrf2 target genes encoding enzymes for stress response and proteasomal subunits, although expression of these genes was not changed significantly in *p45*-null megakaryocytes (see Tables S2 and S3). We surmise that Nrf2 activates these genes in *p45*-null megakaryocytes. In contrast, expression levels of platelet genes were decreased in *p45*-null megakaryocytes, indicating that other CNC proteins cannot compensate at these loci. It is instructive to consider potential differences in transcriptional regulatory mechanisms at genes exclusively activated by p45 versus those coregulated by p45 and Nrf2. No overt differences emerged from the sequence comparison of p45 ChIP-Seq peaks and their flanking regions assigned to the genes that were downregulated in *p45*-null megakaryocytes versus those whose expression was unaffected by p45 deficiency.

As we have identified *Selp* as a direct p45 target gene, p45 functions to control platelet function. This notion is supported by previous reports demonstrating the involvement of p45 in platelet function. $p45^{-/-}$ platelets were largely nonresponsive to thrombin and phorbol myristate acetate when the response was monitored by the surface exposure of P-selectin (62). Since P-selectin is encoded by *Selp*, which is directly activated by p45, the reduction in the surface exposure of P-selectin in *p45*-null platelets with stimulatory factors may result, in part, from a reduced expression level of P-selectin protein per platelet. Another study that used mature megakaryocytes for the analysis of signal transduction demonstrated that integrin αIIbβ3 signaling is dramatically impaired in $p45^{-/-}$ megakaryocytes, which was monitored by the binding of fibrinogen to αIIbβ3 on the surfaces of megakaryocytes (63). Because the protein expression of αIIbβ3 was shown to be comparable between the two genotypes, the reduced fibrinogen binding to $p45^{-/-}$ megakaryocytes appeared to be attributable to the defective signal transduction and insufficient conformational change of αIIbβ3. Among the p45 target gene candidates identified in this study, Pdia6/ERP5 and Ptprj/CD148 are required for integrin αIIbβ3 signaling during platelet activation (64, 65). The reduced expression of these genes may cause the impairment of integrin αIIbβ3 signaling in p45 deficiency.

An important function of platelets under pathological conditions is the promotion of cancer metastasis (56). The critical requirement of platelets themselves for the lung metastasis was demonstrated by the almost complete inhibition of the metastasis in *p45*-null mice, characterized by a major reduction in circulating platelets (4). The results obtained from analyzing $p45^{-/-}$:p45-Tg mice demonstrate that p45 expression in erythromegakaryocytic lineages is required for lung metastasis, further supporting an important contribution of platelets to the development of lung metastasis. Several mechanisms have been proposed for how platelets promote metastasis: protection of cancer cells from immune surveillance, facilitation of interaction between cancer cells and the endothelium, and promotion of tumor growth by secreting

growth factors (6, 66, 67). Platelet surface proteins, such as P-selectin (6), GPVI (5), GPIb (68), PAR4 (4), and GPIIb-IIIa (69), are required for the high incidence of experimental lung metastasis. We have identified *Selp* as a direct target gene of p45 and observed the decreased expression of *Selp* (encoding P-selectin) in $p45^{-/-}$:ΔNTD-Tg megakaryocytes (Fig. 3A) (17). Our analysis also revealed reduced P-selectin levels upon thrombin stimulation and defective aggregation of $p45^{-/-}$:ΔNTD-Tg platelets compared to the WT. These results suggested that $p45^{-/-}$:ΔNTD-Tg platelets are defective in metastasis-promoting activities. As we expected, lung metastasis of melanoma cells was inhibited in $p45^{-/-}$:ΔNTD-Tg mice (Fig. 5). Because circulating platelets are present in $p45^{-/-}$:ΔNTD-Tg mice, suppression of metastasis can be attributed, at least in part, to platelet hypofunction resulting from reduced p45 activity. Therefore, p45 is responsible for conferring normal platelet production and for establishing normal platelet function *in vivo*.

## ACKNOWLEDGMENTS

We thank Shogo Yamamoto and Shuichi Tsutsumi for support in deep sequencing. We also thank Kyowa Hakko Kirin, Co. Ltd., for providing recombinant TPO and the Biomedical Research Core of the Tohoku University Graduate School of Medicine for technical support. We particularly appreciate the assistance of Eriko Naganuma with mouse breeding.

This work was supported by NIH grant DK50107 (E.H.B.), NWO grant 863.09.012 (L.G.), Grants-in-Aid for Scientific Research (M.Y. and H.M.) from the JSPS, Grants-in-Aid for Scientific Research on Innovative Areas (M.Y. and H.M.) from the MEXT, the Tohoku University Global COE for the Conquest of Signal Transduction Diseases with Network Medicine (M.Y.), the Core Research for Evolutional Science and Technology from the JST (M.Y. and H.M.), a research grant from Tohoku University International Advanced Research and Education Organization (R.F.), a research resident fellowship from the Foundation for Promotion of Cancer Research (Japan) for the 3rd Term Comprehensive 10-Year Strategy for Cancer Control (H.S.), and a research grant from the Princess Takamatsu Cancer Research Fund (09-24118) (H.M.).

## REFERENCES

1. **Zucker MB, Nachmias VT.** 1985. Platelet activation. Atherosclerosis **5:**2–18.
2. **Anfossi G, Russo I, Trovati M.** 2009. Platelet dysfunction in central obesity. Nutr. Metab. Cardiovasc. Dis. **19:**440–449.
3. **Boilard E, Nigrovic PA, Larabee K, Watts GF, Coblyn JS, Weinblatt ME, Massarotti EM, Remold-O'Donnell E, Farndale RW, Ware J, Lee DM.** 2010. Platelets amplify inflammation in arthritis via collagen-dependent microparticle production. Science **327:**580–583.
4. **Camerer E, Qazi AA, Duong DN, Cornelissen I, Advincula R, Coughlin SR.** 2004. Platelets, protease-activated receptors, and fibrinogen in hematogenous metastasis. Blood **104:**397–401.
5. **Jain S, Russell S, Ware J.** 2009. Platelet glycoprotein VI facilitates experimental lung metastasis in syngenic mouse models. J. Thromb. Haemost. **7:**1713–1717.
6. **Kim YJ, Borsig L, Varki NM, Varki A.** 1998. P-selectin deficiency attenuates tumor growth and metastasis. Proc. Natl. Acad. Sci. U. S. A. **95:**9325–9330.
7. **Lang PA, Contaldo C, Georgiev P, El-Badry AM, Recher M, Kurrer M, Cervantes-Barragan L, Ludewig B, Calzascia T, Bolinger B, Merkler D, Odermatt B, Bader M, Graf R, Clavien PA, Hegazy AN, Löhning M, Harris NL, Ohashi PS, Hengartner H, Zinkernagel RM, Lang KS.** 2008. Aggravation of viral hepatitis by platelet-derived serotonin. Nat. Med. **14:**756–761.
8. **Lesurtel M, Graf R, Aleil B, Walther DJ, Tian Y, Jochum W, Gachet C, Bader M, Clavien PA.** 2006. Platelet-derived serotonin mediates liver regeneration. Science **312:**104–107.
9. **Nurden AT.** 2011. Platelets, inflammation and tissue regeneration. Thromb. Haemost. **105**(Suppl. 1):S13–S33.
10. **Tripodi A, Anstee QM, Sogaard KK, Primignani M, Valla DC.** 2011. Hypercoagulability in cirrhosis: causes and consequences. J. Thromb. Haemost. **9:**1713–1723.
11. **Zwicker JI, Furie BC, Furie B.** 2007. Cancer-associated thrombosis. Crit. Rev. Oncol. Hematol. **62:**126–136.
12. **Banks RE, Forbes MA, Kinsey SE, Stanley A, Ingham E, Walters C, Selby PJ.** 1998. Release of the angiogenic cytokine vascular endothelial growth factor (VEGF) from platelets: significance for VEGF measurements and cancer biology. Br. J. Cancer **77:**956–964.
13. **Boucharaba A, Serre CM, Grès S, Saulnier-Blache JS, Bordet JC, Guglielmi J, Clézardin P, Peyruchaud O.** 2004. Platelet-derived lysophosphatidic acid supports the progression of osteolytic bone metastases in breast cancer. J. Clin. Investig. **114:**1714–1725.
14. **Labelle M, Begum S, Hynes RO.** 2011. Direct signaling between platelets and cancer cells induces an epithelial-mesenchymal-like transition and promotes metastasis. Cancer Cell **20:**576–590.
15. **Igarashi K, Kataoka K, Itoh K, Hayashi N, Nishizawa M, Yamamoto M.** 1994. Regulation of transcription by dimerization of erythroid factor NF-E2 p45 with small Maf proteins. Nature **367:**568–572.
16. **Mosser EA, Kasanov JD, Forsberg EC, Kay BK, Ney PA, Bresnick EH.** 1998. Physical and functional interactions between the transactivation domain of the hematopoietic transcription factor NF-E2 and WW domains. Biochemistry **37:**13686–13695.
17. **Takayama M, Fujita R, Suzuki M, Okuyama R, Aiba S, Motohashi H, Yamamoto M.** 2010. Genetic analysis of hierarchical regulation for Gata1 and NF-E2 p45 gene expression in megakaryopoiesis. Mol. Cell. Biol. **30:**2668–2680.
18. **Motohashi H, O'Connor T, Katsuoka F, Engel JD, Yamamoto M.** 2002. Integration and diversity of the regulatory network composed of Maf and CNC families of transcription factors. Gene **294:**1–12.
19. **Kimura M, Yamamoto T, Zhang J, Itoh K, Kyo M, Kamiya T, Aburatani H, Katsuoka F, Kurokawa H, Tanaka T, Motohashi H, Yamamoto M.** 2007. Molecular basis distinguishing the DNA binding profile of Nrf2-Maf heterodimer from that of Maf homodimer. J. Biol. Chem. **282:**33681–33690.
20. **Kurokawa H, Motohashi H, Sueno S, Kimura M, Takagawa H, Kanno Y, Yamamoto M, Tanaka T.** 2009. Structural basis of alternative DNA recognition by Maf transcription factors. Mol. Cell. Biol. **29:**6232–6244.
21. **Yamamoto T, Kyo M, Kamiya T, Tanaka T, Engel JD, Motohashi H, Yamamoto M.** 2006. Predictive base substitution rules that determine the binding and transcriptional specificity of Maf recognition elements. Genes Cells **11:**575–591.
22. **Motohashi H, Katsuoka F, Miyoshi C, Uchimura Y, Saitoh H, Francastel C, Engel JD, Yamamoto M.** 2006. MafG sumoylation is required for active transcriptional repression. Mol. Cell. Biol. **26:**4652–4663.
23. **Motohashi H, Fujita R, Takayama M, Inoue A, Katsuoka F, Bresnick EH, Yamamoto M.** 2011. Molecular determinants for small Maf protein control of platelet production. Mol. Cell. Biol. **31:**151–162.
24. **Onodera K, Shavit JA, Motohashi H, Yamamoto M, Engel JD.** 2000. Perinatal synthetic lethality and hematopoietic defects in compound maf-G::mafK mutant mice. EMBO J. **19:**1335–1345.
25. **Shivdasani RA, Rosenblatt MF, Zucker-Franklin D, Jackson CW, Hunt P, Saris CJ, Orkin SH.** 1995. Transcription factor NF-E2 is required for platelet formation independent of the actions of thrombopoietin/MGDF in megakaryocyte development. Cell **81:**695–704.
26. **Lecine P, Villeval JL, Vyas P, Swencki B, Xu Y, Shivdasani RA.** 1998. Mice lacking transcription factor NF-E2 provide in vivo validation of the proplatelet model of thrombocytopoiesis and show a platelet production defect that is intrinsic to megakaryocytes. Blood **92:**1608–1616.
27. **Motohashi H, Katsuoka F, Shavit JA, Engel JD, Yamamoto M.** 2000. Positive or negative MARE-dependent transcriptional regulation is determined by the abundance of small Maf proteins. Cell **103:**865–875.
28. **Chen Z, Hu M, Shivdasani RA.** 2007. Expression analysis of primary mouse megakaryocyte differentiation and its application in identifying stage-specific molecular markers and a novel transcriptional target of NF-E2. Blood **109:**1451–1459.
29. **Deveaux S, Cohen-Kaminsky S, Shivdasani RA, Andrews NC, Filipe A, Kuzniak I, Orkin SH, Roméo PH, Mignotte V.** 1997. p45 NF-E2 regulates expression of thromboxane synthase in megakaryocytes. EMBO J. **16:**5654–5661.
30. **Lecine P, Italiano JE, Kim SW, Villeval JL, Shivdasani RA.** 2000. Hematopoietic-specific beta 1 tubulin participates in a pathway of platelet

biogenesis dependent on the transcription factor NF-E2. Blood **96:**1366–1373.
31. **Tiwari S, Italiano JE, Barral DC, Mules EH, Novak EK, Swank RT, Seabra MC, Shivdasani RA.** 2003. A role for Rab27b in NF-E2-dependent pathways of platelet formation. Blood **102:**3970–3979.
32. **Shavit JA, Motohashi H, Onodera K, Akasaka J, Yamamoto M, Engel JD.** 1998. Impaired megakaryopoiesis and behavioral defects in mafG-null mutant mice. Genes Dev. **12:**2164–2174.
33. **Satoh H, Moriguchi T, Taguchi K, Takai J, Maher JM, Suzuki T, Winnard PT, Raman V, Ebina M, Nukiwa T, Yamamoto M.** 2010. Nrf2-deficiency creates a responsive microenvironment for metastasis to the lung. Carcinogenesis **31:**1833–1843.
34. **Smyth GK.** 2005. Limma: linear models for microarray data, p 397–420. *In* Gentleman R, Carey V, Dudoit S, Irizarry R, Huber W (ed), Bioinformatics and computational biology solutions using R and bioconductor. Springer, New York, NY.
35. **Development Core Team R.** 2012. R: a language and environment for statistical computing. R Foundation for Statistical Computing, Vienna, Austria.
36. **Gentleman RC, Carey VJ, Bates DM, Bolstad B, Dettling M, Dudoit S, Ellis B, Gautier L, Ge Y, Gentry J, Hornik K, Hothorn T, Huber W, Iacus S, Irizarry R, Leisch F, Li C, Maechler M, Rossini AJ, Sawitzki G, Smith C, Smyth G, Tierney L, Yang JY, Zhang J.** 2004. Bioconductor: open software development for computational biology and bioinformatics. Genome Biol. **5:**R80. doi:10.1186/gb-2004-5-10-r80.
37. **Ritchie ME, Silver J, Oshlack A, Holmes M, Diyagama D, Holloway A, Smyth GK.** 2007. A comparison of background correction methods for two-colour microarrays. Bioinformatics **23:**2700–2707.
38. **Smyth GK, Speed TP.** 2003. Normalization of cDNA microarray data. Methods **31:**265–273.
39. **Ritchie ME, Diyagama D, Neilson J, van Laar R, Dobrovic A, Holloway A, Smyth GK.** 2006. Empirical array quality weights for microarray data. BMC Bioinformatics **7:**261. doi:10.1186/1471-2105-7-261.
40. **Smyth GK.** 2004. Linear models and empirical Bayes methods for assessing differential expression in microarray experiments. Stat. Appl. Genet. Mol. Biol. **3:**article 3.
41. **Reiner A, Yekutieli D, Benjamini Y.** 2003. Identifying differentially expressed genes using false discovery rate controlling procedures. Bioinformatics **19:**368–375.
42. **Durinck S, Moreau Y, Kasprzyk A, Davis S, Moor BD, Brazma A, Huber W.** 2005. BioMart and Bioconductor: a powerful link between biological databases and microarray data analysis. Bioinformatics **21:**3439–3440.
43. **Cox AJ.** 2007. ELAND: efficient large-scale alignment of nucleotide databases. lllumina, San Diego, CA.
44. **Zhang Y, Liu T, Meyer CA, Eeckhoute J, Johnson DS, Bernstein BE, Nusbaum C, Myers RM, Brown M, Li W, Liu XS.** 2008. Model-based analysis of ChIP-Seq (MACS). Genome Biol. **9:**R137. doi:10.1186/gb-2008-9-9-r137.
45. **Zhu LJ, Gazin C, Lawson ND, Pagès H, Lin SM, Lapointe DS, Green MR.** 2010. ChIPpeakAnno: a Bioconductor package to annotate ChIP-seq and ChIP-chip data. BMC Bioinformatics **11:**237. doi:10.1186/1471-2105-11-237.
46. **Fejes AP, Robertson G, Bilenky M, Varhol R, Bainbridge M, Jones SJ.** 2008. FindPeaks 3.1: a tool for identifying areas of enrichment from massively parallel short-read sequencing technology. Bioinformatics **24:**1729–1730.
47. **De Cuyper IM, Meinders M, van de Vijver E, de Korte D, Porcelijn L, de Haas M, Eble JA, Seeger K, Rutella S, Pagliara D, Kuijpers TW, Verhoeven AJ, van den Berg TK, Gutiérrez L.** 2013. A novel flow cytometry-based platelet aggregation assay. Blood **121:**e70–e80.
48. **Lan X, Witt H, Katsumura K, Ye Z, Wang Q, Bresnick EH, Farnham PJ, Jin VX.** 2012. Integration of Hi-C and ChIP-seq data reveals distinct types of chromatin linkages. Nucleic Acids Res. **40:**7690–7704.
49. **Dennis G, Sherman BT, Hosack DA, Yang J, Gao W, Lane HC, Lempicki RA.** 2003. DAVID: database for annotation, visualization, and integrated discovery. Genome Biol. **4:**P3. doi:10.1186/gb-2003-4-5-p3.
50. **McLean CY, Bristor D, Hiller M, Clarke SL, Schaar BT, Lowe CB, Wenger AM, Bejerano G.** 2010. GREAT improves functional interpretation of cis-regulatory regions. Nat. Biotechnol. **28:**495–501.
51. **Gilles L, Bluteau D, Boukour S, Chang Y, Zhang Y, Robert T, Dessen P, Debili N, Bernard OA, Vainchenker W, Raslova H.** 2009. MAL/SRF complex is involved in platelet formation and megakaryocyte migration by regulating MYL9 (MLC2) and MMP9. Blood **114:**4221–4232.
52. **Palabrica T, Lobb R, Furie BC, Aronovitz M, Benjamin C, Hsu YM, Sajer SA, Furie B.** 1992. Leukocyte accumulation promoting fibrin deposition is mediated in vivo by P-selectin on adherent platelets. Nature **359:**848–851.
53. **Stenberg PE, McEver RP, Shuman MA, Jacques YV, Bainton DF.** 1985. A platelet alpha-granule membrane protein (GMP-140) is expressed on the plasma membrane after activation. J. Cell Biol. **101:**880–886.
54. **Yokoyama S, Ikeda H, Haramaki N, Yasukawa H, Murohara T, Imaizumi T.** 2005. Platelet P-selectin plays an important role in arterial thrombogenesis by forming large stable platelet-leukocyte aggregates. J. Am. Coll. Cardiol. **45:**1280–1286.
55. **Igarashi K, Itoh K, Motohashi H, Hayashi N, Matuzaki Y, Nakauchi H, Nishizawa M, Yamamoto M.** 1995. Activity and expression of murine small Maf family protein MafK. J. Biol. Chem. **270:**7615–7624.
56. **Gasic GJ, Gasic TB, Galanti N, Johnson T, Murphy S.** 1973. Platelet-tumor-cell interactions in mice. The role of platelets in the spread of malignant disease. Int. J. Cancer **11:**704–718.
57. **Gay LJ, Felding-Habermann B.** 2011. Contribution of platelets to tumor metastasis. Nat. Rev. Cancer **11:**123–134.
58. **Nierodzik ML, Plotkin A, Kajumo F, Karpatkin S.** 1991. Thrombin stimulates tumor-platelet adhesion in vitro and metastasis in vivo. J. Clin. Investig. **87:**229–236.
59. **Kiekhaefer CM, Boyer ME, Johnson KD, Bresnick EH.** 2004. A WW domain-binding motif within the activation domain of the hematopoietic transcription factor NF-E2 is essential for establishment of a tissue-specific histone modification pattern. J. Biol. Chem. **279:**7456–7461.
60. **Chaturvedi CP, Hosey AM, Palii C, Perez-Iratxeta C, Nakatani Y, Ranish JA, Dilworth FJ, Brand M.** 2009. Dual role for the methyltransferase G9a in the maintenance of beta-globin gene transcription in adult erythroid cells. Proc. Natl. Acad. Sci. U. S. A. **106:**18303–18308.
61. **Motohashi H, Kimura M, Fujita R, Inoue A, Pan X, Takayama M, Katsuoka F, Aburatani H, Bresnick EH, Yamamoto M.** 2010. NF-E2 domination over Nrf2 promotes ROS accumulation and megakaryocytic maturation. Blood **115:**677–686.
62. **Levin J, Peng JP, Baker GR, Villeval JL, Lecine P, Burstein SA, Shivdasani RA.** 1999. Pathophysiology of thrombocytopenia and anemia in mice lacking transcription factor NF-E2. Blood **94:**3037–3047.
63. **Shiraga M, Ritchie A, Aidoudi S, Baron V, Wilcox D, White G, Ybarrondo B, Murphy G, Leavitt A, Shattil S.** 1999. Primary megakaryocytes reveal a role for transcription factor NF-E2 in integrin alpha IIb beta 3 signaling. J. Cell Biol. **147:**1419–1430.
64. **Jordan PA, Stevens JM, Hubbard GP, Barrett NE, Sage T, Authi KS, Gibbins JM.** 2005. A role for the thiol isomerase protein ERP5 in platelet function. Blood **105:**1500–1507.
65. **Senis YA, Tomlinson MG, Ellison S, Mazharian A, Lim J, Zhao Y, Kornerup KN, Auger JM, Thomas SG, Dhanjal T, Kalia N, Zhu JW, Weiss A, Watson SP.** 2009. The tyrosine phosphatase CD148 is an essential positive regulator of platelet activation and thrombosis. Blood **113:**4942–4954.
66. **Nieswandt B, Hafner M, Echtenacher B, Mannel DN.** 1999. Lysis of tumor cells by natural killer cells in mice is impeded by platelets. Cancer Res. **59:**1295–1300.
67. **Palumbo JS, Talmage KE, Massari JV, La Jeunesse CM, Flick MJ, Kombrinck KW, Jirousková M, Degen JL.** 2005. Platelets and fibrin(ogen) increase metastatic potential by impeding natural killer cell-mediated elimination of tumor cells. Blood **105:**178–185.
68. **Jain S, Zuka M, Liu J, Russell S, Dent Guerrero JJA, Forsyth J, Maruszak B, Gartner TK, Felding-Habermann B, Ware J.** 2007. Platelet glycoprotein Ib alpha supports experimental lung metastasis. Proc. Natl. Acad. Sci. U. S. A. **104:**9024–9028.
69. **Lonsdorf AS, Krämer BF, Fahrleitner M, Schönberger T, Gnerlich S, Ring S, Gehring S, Schneider SW, Kruhlak MJ, Meuth SG, Nieswandt B, Gawaz M, Enk AH, Langer HF.** 2012. Engagement of αIIbβ3 (GPIIb/IIIa) with αvβ3 integrin mediates interaction of melanoma cells with platelets: a connection to hematogenous metastasis. J. Biol. Chem. **287:**2168–2178.